9

Digital Holographic Microscopy: A New Imaging Technique to Quantitatively Explore Cell Dynamics with Nanometer Sensitivity

Pierre Marquet[1,2] and Christian Depeursinge[3]

[1]*Centre de Neurosciences Psychiatriques, Centre Hospitalier Universitaire Vaudois, Département de Psychiatrie, Switzerland*

[2]*Brain Mind Institute, Institute of Microengineering, École Polytechnique Fédérale de Lausanne, Switzerland*

[3]*Institute of Microengineering, École Polytechnique Fédérale de Lausanne, Switzerland*

9.1 Chapter Overview

In the first part of this chapter, we summarize how the new concept of digital optics, applied to the field of holographic microscopy, has allowed the development of a reliable and flexible digital holographic quantitative phase microscopy (DH-QPM) technique at the nanoscale, particularly suitable for cell imaging. In the second part, particular emphasis is placed on the original biological information provided by the quantitative phase signal. We present the most relevant DH-QPM applications in the field of cell biology, including automated cell counts, recognition, classification, three-dimensional tracking, and discrimination between physiological and pathophysiological states. In addition, we present how the phase signal can be used to specifically calculate some important biophysical cell parameters including dry mass, protein content and production, membrane fluctuations at the nanoscale, absolute volume, transmembrane water permeability, and how these different biophysical parameters can be used to perform a non-invasive multiple-site optical recording of neuronal activity.

Multi-dimensional Imaging, First Edition. Edited by Bahram Javidi, Enrique Tajahuerce and Pedro Andrés.

9.2 Introduction

Historically, optical microscopy has been one of the most productive scientific instruments in technology and medicine. Cells and micro-organisms were identified for the first time in the nineteenth century. These observations can be considered the beginning of developments in modern biology and medicine. On the other hand, some limitations of optical microscopy soon appeared due in particular to the lack of resolution formulated by the well-known Abbe's law, as well as the lack of quantitative information due to the analogical nature of conventional optical microscopes.

Overcoming these limitations is particularly crucial in the field of cell biology, in which to be able to quantitatively appreciate cell structure and dynamics in ever-increasing detail is essential to elucidate the mechanisms underlying physiological or pathological cell processes. In addition, considering that most biological cells differ only slightly from their surroundings in terms of optical properties (including absorbance, reflectance etc.) obtaining a high resolution and quantitative visualization of cell structure and dynamics remains a difficult challenge.

Consequently, several modes of contrast generation have been developed to overcome these limitations. Among the many contrast-generating modes, those based on wavefront phase information, representing an intrinsic contrast of transparent specimens, have demonstrated their relevance for noninvasive visualization of cell structure, in particular the Zernicke's invention of *phase contrast* (PhC) in the mid-twentieth century [1]. Currently, PhC, as well as Normarski's differential interference contrast (DIC), are widely used contrast-generating techniques available for high-resolution light microscopy. In contrast to fluorescence techniques, PhC and DIC allow the visualization of transparent specimens, making visible, in particular, the fine subcellular structural organization without using any staining contrast agent. Basically, these two noninvasive contrast-generating techniques, PhC and DIC, result from their capacity to transform, in detectable modulation intensity, the minute relative phase shift that a transparent microscopic object, differing from the surroundings only by a slight difference of refractive index, induces between the transmitted wave light and the undeviated background wave (PhC) and between two orthogonally polarized transmitted waves (DIC). However, PhC and DIC do not allow the direct and quantitative measurement of phase shift or optical path length. Consequently, DIC or PhC signal variations are only qualitative and remain difficult to interpret in terms of quantitative modification of specific biophysical cell parameters.

In contrast, interference microscopy has the capacity to provide a direct measurement of the optical path length based on interference between the light waves passing the specimen, called the *object wave*, and *reference wave*. Although quantitative phase measurements with interference microscopy applied to cell imaging were already known in the 1950s, since the seminal work of Barer [2] only a few attempts have been reported to dynamically image live cells in biology [3]. Indeed phase shifts are very sensitive to experimental artifacts, including lens defects, and noise originating from vibrations or thermal drift. Temporal phase shifting interferometry therefore requires demanding and costly opto-mechanical designs preventing wider applications in biology.

In parallel, holography techniques were developed by Gabor in 1948 [4] who demonstrated its lensless imaging capabilities thanks to the reconstruction of an exact replica of the full wavefront (amplitude and phase) emanating from the observed specimen (object wave). Due to costly opto-mechanical designs and the non-availability of long coherence sources in optics, few applications were developed at that time.

Among the many contrast-generating mode, fluorescence microscopy in a confocal configuration (confocal fluorescent lasers canning microscopy, CLSM) and its extension to multiphoton fluorescent excitation for a few decades has been a powerful and widely used cellular imaging technique in biology [5,6].

Nowadays, the chance to bring quantitative and specific data in optical microscopy on one hand, and to reach the nanometer scale on the other, appears more and more clearly to be an incentive to invent and develop new concepts in optical microscopy. Most of them call for the new means offered by informatics and algorithmics. Indeed, optical data are now increasingly easily and rapidly processed, bringing an important push to new applications, improved performance, and reproducibility of scientific results. Practically, the development of quantitative microscopy helps much in extracting meaningful data from images. More generally, the quantitative evaluation of an increasing number of parameters extracted from microscopic images including phase, fluorescence, or nonlinear images such as second (SHD) [7] and third harmonics (THD), or even *Coherent Anti-Stokes* Raman Scattering (CARS) [8], are at the basis of a new field of investigation, sometime called *bio-image informatics*. A clear trend towards super-resolution microscopy is another strand in the revival of optical microscopy [9]. It is the fruit of better knowledge about the physical principles underlying microscopy. The use of coherence properties of light waves has, henceforth, altogether permitted breaking the diffraction limit and providing a full 3D image of microscopic or nanometric objects. Super-resolution is a commonly accepted term to designate in optical microscopy allowing the imaging of objects beyond the diffraction limit (defined by Abbe's law).

Practically, interferences created by partially coherent waves allow structuring of light beams: fringes are generated for SIM (*Structured Illumination Microscopy*) whereas a combination of focal spots is used for STED (*STimulated Emission Depletion microscopy*) and GSD (*Ground State Depletion microscopy*). These beam structuring techniques are used to enlarge the bandpass of the image beyond the bandpass of the *microscope objective* itself. These new super-resolution are all based on fluorescence imaging of natural or selected fluorophores. Most of them (except SIM) exploit the nonlinear response of fluorescent dyes or proteins to extend further the spectral domain of the images, thereby permitting the achievement of super-resolved images.

The use of statistical treatment of optical signals is a complimentary approach to improve the localization of single fluorescent molecules and thereby push the resolution beyond the diffraction limit [10]. Palm, Storm, and derived methods are examples of that approach. Resulting from fluorescent tag availability, these methods are priceless in biology. However, they do not provide any information about the dielectric properties of specimens, which also give access to important biophysical parameters. Practically, these dielectric properties can be efficiently detected using new digital interferometric and/or holographic approaches.

Indeed, in the field of holography and interferometry, scientific advances lowering the cost of lasers and data acquisition equipment, as well as the development of computing facilities, the large spread of PCs and digital signal processors, have completely changed perspectives. Practically, this led to the development of various quantitative phase microscopy (QPM) approaches related to holography [11–41], interferometry [42–78] being considerably simpler to implement than classical interference microscopy, while providing a reliable and quantitative phase mapping of the observed specimen. It may be noted that QPM techniques based on other approaches, including transport-intensity equations [79,80], quadriwave lateral shearing

interferometer [81] or phase-retrieval algorithmic [82–85], have also been developed. Finally, we note some attempts to use DIC and PhC as quantitative imaging techniques [86–92].

In the first part of this chapter, we present the principle of classical holography as well as the current state-of-the-art in digital holography microscopy. Emphasis is given to the key benefits provided by digital means to develop a reliable and flexible quantitative phase microscopy technique with a nanometric axial sensitivity. In a second part, the most relevant applications in the field of cell biology provided by *digital holographic quantitative phase microscopy* (DH-QPM) are presented. Particular attention is paid to how specific biophysical cell parameters can be determined from the quantitative phase signal and how such parameters can be used to address important biological questions, including the optical monitoring of neuronal activity.

9.3 Holographic Techniques

9.3.1 Classical Holography

Holography techniques were developed by Gabor in 1948 with the aim of improving the detection of spatial resolution in the X-ray wavelength by exploiting its lensless imaging capabilities [93]. This resulted in the possibility of generating, during the illumination of the recorded hologram (reconstruction process), an exact replica with a specific magnification of the full object wavefront created by the observed specimen [94,95]. However, as already identified by Gabor, the imaging possibilities of holography are greatly reduced in quality owing to the presence of different diffraction orders in the propagation of the diffracted wavefront by the hologram when illuminated during the reconstruction process. This was resolved by Leith and Upatneik, who proposed the use of a reference wave from a slightly different propagation direction than the object wave [96,97]. This method, referred to as *off-axis geometry*, has been analyzed from a computational point of view [98] with a formalism based on diffraction, and was the first to use quantitative phase measurements [99]. Practically, the first developments in off-axis configuration were performed through a common-path configuration due to the coherence limitation of the light sources. Moreover, the emergence of laser light sources, enabling very long coherence lengths with high power, takes advantage of the versatility of "interferometric configuration". Note that short coherence length sources have been investigated recently in various cases [73,100,101]. Shorter coherence lengths have the capability to improve the lateral resolution as well as to decrease the coherence noise, which could limit the quality of the reconstructed image, particularly the phase sensitivity. However, these low coherence implementations require more complicated arrangements where the coherence zone (in both spatial and temporal domains) must be adapted to ensure optimal interference [102].

9.3.2 From Classical to Digital Holography

The use of digital means in holography gradually occurred at the end of the 1960s when Goodman used a vidicon detector to encode a hologram, which could be reconstructed on a computer [103]. However, the interest in digital holography rose with the availability of cheaper digital detectors and charge-coupled device (CCD) cameras. The use of CCD cameras for holographic applications was validated in the mid-1990s in the case of reflection macroscopic holograms [104], and microscopic holograms in endoscopic applications [105]. Another approach to

hologram reconstruction was developed by taking advantages of the capability of digital detectors to rapidly record multiple frames, through the use of a phase-shifting technique [14] as developed first for interferometry [106,107]. Up to this point, holography was essentially considered an imaging technique, enabling the possibility of lensless imaging or the capability of focusing images recorded out of focus through the recovery of the full wavefront. The digital treatment, contrary to the classical approach, considered the wavefront to be a combination of amplitude and phase, which led to the development of quantitative phase imaging through holography [13].

9.3.3 Digital Holography Methods

The two main approaches to recovering the object wave are namely *temporal decoding*, that is, phase shifting, and *spatial decoding*, that is, off-axis methods. Phase shifting reconstruction methods are based on the combination of several frames, which enables the suppression of the zero order and one of the cross terms through temporal sampling [108,109]. The most well-known phase-shifting algorithm, proposed by Yamaguchi [14], is based on the recording of four frames separated by a phase shift of a quarter of a wavelength. Various combinations of frames derived from interferometry have been considered [107,108] and many different approaches have been developed to produce the phase shift, including high precision piezo-electric transducers that move a mirror in the reference wave, or acousto-optics modulators using the light frequency shift, and so on. One of the main issues in the phase shifting method is the requirement of several frames for reconstruction in interferometric setups, which are commonly very sensitive to vibrations, so it could be difficult to ensure stable phase shifts and an invariant sample state during acquisition. In addition, the requirements on the accuracy of the phase-shifts are rather high with regard to displacements in the magnitude of hundreds of nanometers, implying the use of high-precision transducers. Consequently, several attempts were made to either reduce the required number of frames for reconstruction, which led to two-frame reconstruction [110,111], or to enable the recoding of the various phase shift frames simultaneously by employing, for example, multiplexing methods [112]. On the other hand, more refined algorithms were developed in order to loosen the accuracy requirements of phase shift methods [113–115].

The second main approach to recovering the object wave is based on an off-axis configuration, so that the different diffraction terms encoded in the hologram (zero-order wave, real image, and virtual image) propagate in different directions, enabling their separation for reconstruction. This configuration was the one employed for the first demonstration of a fully numerical recording and reconstruction holography [105,116].

In practice, reconstruction methods based on off-axis configuration usually rely on Fourier methods to filter one of the diffraction terms. This concept was first proposed by Takeda *et al*. [117] in the context of interferometric topography. The method was later extended for smooth topographic measurements for phase recovery [118], and generalized for use in digital holographic microscopy with amplitude and phase recovery [13]. As discussed in the following paragraph, the main characteristic of this approach is its capability of recovering the complex object wave through only one acquisition, thus greatly reducing the influence of vibrations. However, as the diffraction terms are spatially encoded in the hologram, this one-shot capability potentially comes at the cost of usable bandwidth. In addition, frequency modulation,

induced by the angle between the reference and the object wave, has to guarantee the separability of the information contained in the different diffraction terms that are encoded in the hologram, while carrying a frequency compatible with the sampling capacity of digital detectors.

9.3.4 Digital Holographic Microscopy

9.3.4.1 State-of-the-Art

The applications of digital holography to microscopy are characterized by the fact that the wavefront diffracted by the microscopic specimen is acquired and reconstructed in a numerical form. The innovative aspects of digital holographic microscopy reside in the fact that there is no need for focusing before image acquisition. Compared to the acquisition of the formed image, hologram acquisition with a digital camera appears more flexible and "information rich". The result of this holographic approach is a new microscope that we have called the *Digital Holographic Microscope* (DHM) [13,119]. It comprises a microscope objective to adapt the sampling capacity of the camera to the information content of the hologram, enabling reconstruction of the complex 3D wavefront scattered by the microscopic specimen (see Fig. 9.1b later). DHM delivers the data describing the complex wavefront that can be extracted directly from the digitalized hologram. This set of complex numbers is then propagated to the image plane of the specimen, thereby restoring the true magnified image of the object. The complex data provided by the numerical reconstruction of the wavefront opens the way to the possibility of fully simulating light wave propagation and conditioning by numerical methods, correcting aberrations, and distortions, thereby avoiding the complexity of an optical setup to achieve the necessary beam manipulations [120–123]. In many ways, the introduction of numerical procedures to mimic complex optical systems represents a breakthrough in modern optics [124]. This modality allows for subsequent reconstruction and focusing of the intensity or quantitative phase image. Practically, the propagated wavefront delivers the distribution of the image in depth and therefore allows for extension of the depth of focus without resorting to complex optical realizations [125]. Moreover the high-sensitivity phase measurement provided by the reconstructed wavefront, resulting from an interferometric detection, permits the evaluation of optical path lengths with ultrahigh resolution, in practice down to the subnanometer scale, depending on wavelength and other parameters that include the integration time. Such a wavefront reconstruction can be achieved in real time with a personal computer, the hologram being recorded with a digital camera.

Optical Set-up: A digital holographic microscope [126] consists of both an optical setup devoted to hologram formation and software specially developed to process numerically the digitized hologram. The hologram results from the interference of the object beam with a reference wave that can be kept separate from the object beam. The reference beam is controllable both in intensity and polarization in order to optimize the contrast and signal. The goal is to estimate precisely the propagated wavefront corresponding to either the virtual or real image of the specimen magnified by the microscope objective. Computing the wavefront at various positions along the beam by progressively increasing the reconstruction distance will yield the three-dimensional distribution of the wavefront. Different optical setups have been proposed to perform microscopy with holography [127–129]. We have given preference to optical setups making use of a microscope objective offering the largest numerical apertures [13]. Typical

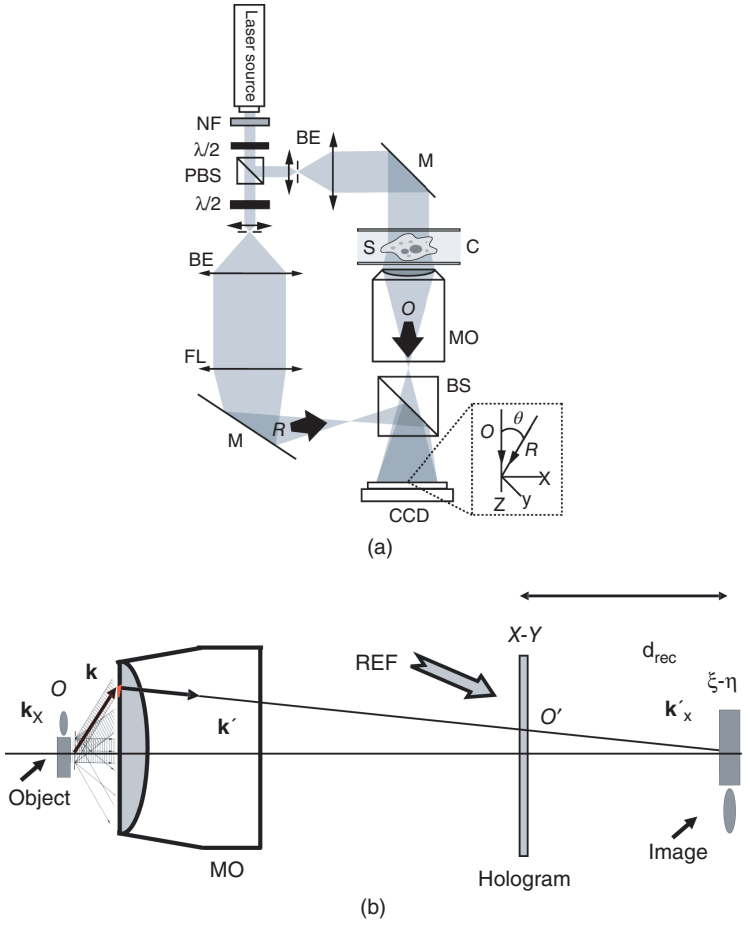

Figure 9.1 Optical setup: (a) for transmission DHM, (b) role of the microscope objective (MO): Magnifying the image of the specimen so that the hologram can be sampled by an electronic camera according to Shannon's rules. *O*: object beam, *R*: reference beam, BS: Beam splitter, PBS: polarizing beam splitter, M: Mirrors, CCD: camera, MO: Microscope objective, NF: neutral filter; $\lambda/2$: half wave plate, FL: field lens; S: specimen; C: specimen chamber. *Insets*: details showing off-axis geometry at the incidence on the CCD. *Source*: Marquet, P., Depeursinge, C., Magistretti, P.J., 2013, Neural cell dynamics explored with digital holographic microscopy, Annual Review of Biomedical Engineering, (15), 407–431

arrangements developed and used by us for exploring cell structure and dynamics is depicted in Fig. 9.1(a): DHM allows the recording of a digital hologram corresponding to the wave scattered by the specimen in a transmission configuration by means of a standard CCD (or CMOS) camera inserted at the exit of a Mach–Zehnder interferometer.

Other configurations are possible, depending on the targeted application, but will not be reviewed in detail here. An important issue is the need for a reference beam, which should be controllable both in intensity and polarization. Contrast and signal could be accordingly improved. The holographic principle also permits other valuable concepts to be built on: In particular the possibility of superimposing several holograms. Holograms with several reference

waves corresponding to several polarization states can be generated in order to analyze the birefringence properties of specimens: strained dielectrics or biological molecules [130,131]. Reference waves corresponding to different wavelengths can also be generated, permitting the use of synthetic wavelengths from a single hologram [132].

Reconstruction: As in other developments in digital holography, the reconstruction method is based on the theory of diffraction. Intercepting the wavefront provided by the microscope objective (MO) at finite distance from the specimen image plan gives rise to holograms in the Fresnel zone. Huyghens–Fresnel expression of diffraction will therefore be considered as valid for the calculation of the propagation of the reconstructed wave.

The (MO) allows us to adapt the object wavefield to the sampling capacity of the camera: the lateral components of the wavevector $k_{x \text{ or } y}$ can be divided by the magnification factor M of the MO, therefore permitting an adequate sampling of the off-axis hologram interference fringes by the electronic camera (Fig. 9.1b).

The hologram taken after the MO results from the superposition of the object wave O' generated by the MO from the wavefield O, emitted by the specimen and a reference wave R, having some non-cancelling mutual coherence with O'. Practically, the hologram intensity is given by expression (9.1):

$$I_H(x,y) = (R + O')^* \cdot (R + O') = |R|^2 + |O'|^2 + R^* O' + R O'^* \tag{9.1}$$

As is usual in holography, the reconstruction of the wavefront can be achieved in the plane of the hologram by illuminating it with a wave matching the reference wave. Taking advantage of a full digital approach, the reconstruction of the object wavefront can be fully achieved by a computer calculating the diffraction process of a simulated reference wave R_{num} by the hologram intensity distribution. Then the distribution of the object wave front in space is obtained by calculating the propagation of the object wavefront reconstructed in the plane of the hologram. As is well known by holographers, the reconstruction of the wavefront gives rise to several propagated beams, the zero order beam and higher order beams, mainly in the order of $+1$ and -1. These two orders provide virtual and real images that appear as twin images, which are the reflection of one another about the hologram plane. If the reference wave is "on axis", that is, propagating in parallel to the object wave O', propagated real and virtual images appear as superposed on any plane where the reconstruction is performed. The specimen image appears therefore as "blurred" by the presence of the unfocused twin image. In order to eliminate this blur, filtration must be performed to eliminate all scattered beam except one: In those conditions focused virtual (O'*) and/or real (O') images can be reconstructed exactly.

Concretely, the reconstruction method is based on the restoration of the object wavefield O'_{rec}. The reconstruction or restoration of the object wavefield O'_{rec} is usually achieved in the hologram plane x-y by forming the product of the hologram intensity with the reference wave R_{num} generated in the computer and further adjusted to match the original reference wave:

$$O'_{rec}(x,y) = I_{H\ filtered}(x,y) \cdot R_{num}(x,y) / |R_{num}|^2 \tag{9.2}$$

Practically, hologram $I_H(x,y)$ filtering allows us to isolate one of the cross terms RO'^* *or* R^*O' appearing in Eq. (9.1). Filtering can be achieved either in the time domain or in the space domain.

In the time domain several phase shifted holograms (at least three, but usually four) are taken successively in order to eliminate the square part in Eq. (9.1) corresponding to the zero-order

term and one of the cross terms corresponding to the virtual image. Time domain filtering is similar to the so-called "phase-shifting interferometry" and has been proposed by Yamaguchi [14,133] for application in holography. Although this method has the advantage of preserving the full spatial bandwidth, a major inconvenience is that multiple holograms must be taken; a fact that renders the reconstruction of movement blurred and instantaneous images difficult to take.

In the space domain, the filtering of cross terms can be achieved by taking a digitalized hologram in a slightly off-axis geometry [126]. Off-axis geometry introduces a spatial carrier frequency and demodulation restores the full spatial frequency content of the wavefront. The main advantage of this approach is that all the information for reconstructing the complex wavefield comes from a single hologram [13]. In microscopy the full bandwidth of the beam delivered by the MO can be acquired without limitation.

Finally, selecting the signal corresponding to the third term in Eq. (9.1) in the Fourier domain of the hologram [134] allows for the full restoration of the wavefront O'. Reconstructing the wavefront in 3D is therefore simply done by propagating the wavefront generated in the hologram plane x-y to the object plane $\xi-\eta$, which is situated at the distance d_{rec}. This can be simply achieved by computing the Fresnel transform of the wavefield. The mathematical expression Eq. (9.3) used for that computation is:

$$O'(\xi,\eta) = -i \cdot \exp(ikd_{rec}) \cdot \boldsymbol{F}^{\sigma}_{Fresnel}[O'(x,y)], \tag{9.3}$$

which, in the paraxial approximation, can be put in the following form that is computed after discretization.

$$\boldsymbol{F}^{\sigma}_{Fresnel}\left[O'(x,y)\right] = \frac{1}{\sigma^2}\exp\left[\frac{i\pi}{\sigma^2}\left(\xi^2+\eta^2\right)\right] \cdot \boldsymbol{F}_{Fouirer}\left\{O'(x,y)\cdot\exp\left[\frac{i\pi}{\sigma^2}\left(x^2+y^2\right)\right]\right\} \tag{9.4}$$

with

$$\sigma = \sqrt{\lambda d_{rec}} = \sqrt{2\pi\frac{d_{rec}}{k}}. \tag{9.5}$$

When the reconstruction distance d_{rec} approaches infinity, the parameter σ also tends to infinity and the Fresnel transform becomes identical to Fourier transform.

In our DHM implementation, there is no time spent heterodyning or moving mirrors. The microscope design is therefore simple and robust. DHM brings quantitative data derived simultaneously from the amplitude and the quantitative phase of the complex reconstructed object wavefront.

Our approach requires the adjustment of several reconstruction parameters [13], which can done using a computer-aided method developed by our group. Some image processing is also needed to improve the accuracy of the phase [135]. Using a high numerical aperture, submicron transverse resolution has been achieved: to 300 nm lateral resolution, which corresponds to diffraction limited resolution. Accuracies of approximately 0.1° have been estimated for phase measurements. In reflection geometry, this corresponds to a vertical resolution less than 1 nm at a wavelength of 632 nm. In the transmission geometry, the resolution is limited to a few nanometers as far as living cells are concerned.

Characterization of the effect of noise on the formation of the hologram and the reconstruction of the image results in an improved signal-to-noise ratio by the coherent detection of low level of scattered light [136,137]. This improvement is often described as "coherent amplification" of the signal.

9.4 Cell Imaging with Digital Holographic Quantitative Phase Microscopy

Biological specimens such as living cells and tissues are usually phase objects; that is, they are transparent and made visible most often by PhC as explained earlier. The phase signal originates in the RI difference generated by the presence of organic molecules in cells, including proteins, DNA, organelles, and nuclei. Consequently, DH-QPM visualizes cells by quantitatively providing the phase retardation that they induce on the transmitted wavefront [15]. This quantitative phase signal is given by the following expression:

$$\Phi = \frac{2\pi}{\lambda}(\overline{n}_c - n_m)d, \tag{9.6}$$

where d is the cellular thickness, $\overline{n}_c$ is the intracellular RI averaged over the OPL of optical rays crossing the specimen, and n_m is the RI of the surrounding medium.

DH-QPM allows for the precise determination of the phase or OPL, directly proportional to the (RI) integrated over the propagation of the light beam. Point-to-point OPL determinations yield an absolute PhC image in microscopy, and very high accuracies, comparable to those provided by high-quality interferometers, can be achieved. However, DH-QPM offers much-improved flexibility as well as the capability to adjust the reference plane with a computer (i.e., without positioning the beam or the object). A quantitative phase image, obtained for living neurons in culture, is presented in Fig. 9.2(b) (Plate 16).

9.4.1 Cell Counting, Recognition, Classification, and Analysis

Several original applications made with DH-QPM, in combination with the unique possibilities presented by digital optics (real-time imaging, extended depth of focus, etc.), in the field of cell imaging are presented next.

The DHM-QP modality offers a quantitative alternative to classical PhC and DIC. Practically, the quantitative phase signal is particularly well suited to the development of algorithms, based on biophysical cell parameters, allowing automated cell counting [16,17,138,139], recognition, and classification [18,19,21,140–143]. Considering the fact that the quantitative phase signal also provides some information about the intracellular content, which contributes to modifying the intracellular RI, interesting applications allowing discrimination between physiological and pathophysiological states have been achieved, particularly in the fields of assisted reproduction [20,22,144] and cancer research [23,24,61]. For example, proposing that quantitative evaluation of the phase shift recorded by DHM-QP could provide new information on the structure and composition of the sperm head or cell nucleus has been useful to clinical practice.

The ability of digital propagation to apply autofocusing [25–27] and extended depth of focus [28–30,125] has opened up the possibility of efficiently tracking particles [31,145,146] including those capable of second harmonic generation [147,148]. In addition, applications to the study of cell migration in 3D have been made [18,25,32,33,35,149–151] offering an alternative to the shallow depth of field of conventional microscopy, which hampers any fast 3D tracking of cells in their environment.

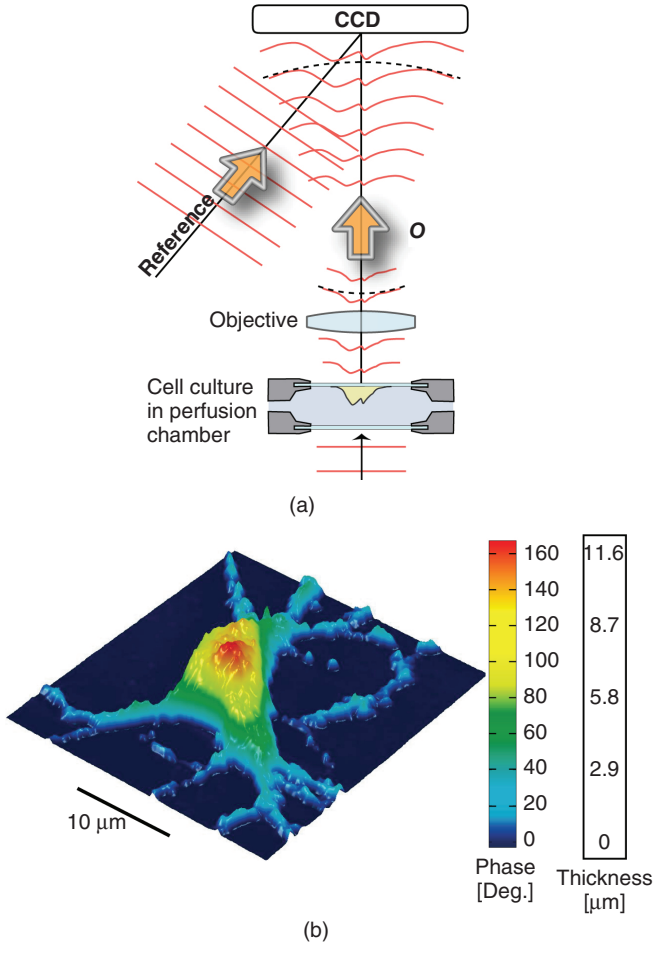

Figure 9.2 (Plate 16) Digital holographic microscopy (DHM) of living mouse cortical neurons in culture. (a) Schematic representation of cultured cells mounted in a closed perfusion chamber and trans-illuminated (b) 3D perspective image in false colors of a living neuron in culture. Each pixel represents a quantitative measurement of the phase retardation or cellular optical path length (OPL) induced by the cell with a sensitivity corresponding to a few tens of nanometers. By using the measured mean value of the neuronal cell body refractive index, resulting from the decoupling procedure, scales (*right*), which relate OPL (°) to morphology in the *z*-axis (µm), can be constructed. *See plate section for the color version*

9.4.2 Dry Mass, Cell Growth, and Cell Cycle

As described earlier, the measured quantitative phase shift induced by an observed cell on the transmitted light wavefront is proportional to the intracellular RI, which mainly depends on protein content. Therefore, this measure can be used to directly monitor protein production,

owing to a relation established more than 50 years ago by Barer [2,152]. Within the framework of interference microscopy, the phase shift induced by a cell is related to its dry mass (DM) by the following equation (converted to the International System of Units):

$$DM = \frac{10\lambda}{2\pi\alpha} \int_{S_c} \Delta\varphi ds = \frac{10\lambda}{2\pi\alpha} \Delta\overline{\varphi} S_c, \tag{9.7}$$

where $\Delta\overline{\varphi}$ is the mean phase shift induced by the whole cell, λ is the wavelength of the illuminating light source, S_c is the projected cell surface, and α is a constant known as the specific refraction increment (in cubic meters per kilogram) and related to the intracellular content. α is approximated by $1.8–2.1 \times 10^{-3}$ m^3 kg^{-1} when considering a mixture of all the components of a typical cell.

Recently, several groups using various QPM techniques have begun to exploit this phase/DM relationship to study the dynamics of cell growth and the cell cycle [36,153–156]. The relationship has also been explicitly and implicitly used to calculate hemoglobin content in red blood cells (RBCs) [157–161].

9.4.3 Cell Membrane Fluctuations and Biomechanical Properties

RBCs are squeezed as they pass capillaries often smaller than their cell diameter. This ability can be attributed to the remarkable elastic properties of the membrane structure. This structure exhibits a high resistance to stretching ensuring that no leakage through the lipid bilayer occurs, whereas its low resistance to bending and shearing allows the cell to easily undergo morphological changes when passing through small capillaries. As a consequence of these elastic properties, RBCs show spontaneous cell membrane fluctuations (CMFs) at the nanometric scale, often called flickering. Owing to their high sensitivity, and allowing us to quantitatively measure RBC membrane fluctuations over the whole cell surface, different QPM techniques have shed new light on these CMFs by providing quantitative information about the biomechanical properties of RBC membranes [37,52,68,69,161,1621]. We also should mention the integration of DHM with optical tweezers, which is a very promising tool, especially with respect to monitoring trapped objects along the axial direction as well as manipulating and testing biomechanical properties of cells [18,38,163–165].

9.4.4 Absolute Cell Volume and Transmembrane Water Movements

The various applications presented previously highlight the wealth of information brought by the phase signal regarding cell dynamics. However, as indicated by Eq. (9.1), information concerning the intracellular content related to $\overline{n}_c$ is intrinsically mixed with morphological information relating to a thickness d. As a result of this dual dependence, the phase signal remains difficult to interpret. As an illustration, a simple hypotonic shock induces an *a priori* surprising phase signal decrease [39] that is difficult to interpret as cellular swelling, resulting coherently, however, from a decrease of $\overline{n}_c$ due to dilution of the intracellular content by an osmotic water influx. Accordingly, some strategies have been developed to separately measure cell morphology and RI. Some authors [166,167] measured the intracellular RI by trapping cells between two cover slips separated by a known distance. However, this approach, which prevents cell

movement, precludes the possibility of exploring dynamic cellular processes. Recently, spectroscopy phase microscopy approaches [134–136] have addressed this deficiency, at least as far as cells with high intrinsic dispersion properties are considered, including RBCs (owing to presence of the hemoglobin pigment). However, such spectroscopy approaches are applicable only to a very limited variety of cell types, most of which have intrinsic dispersions almost identical to that of water. We have developed another approach, called the decoupling procedure, to separately measure the parameters $\overline{n}_c$ and d from the phase signal Φ, based on a modification of the extracellular RI n_m. Basically, this method consists of performing a slight alteration of the extracellular RI n_m and recording two holograms that correspond to the two different values of n_m, thereby allowing reconstruction of two quantitative phase images (Φ_1 and Φ_2) described, for each pixel i, by the following system of equations:

$$\Phi_{1,i} = \frac{2\pi}{\lambda_1}(\overline{n}_{c,i} - n_{m,1})d_i \tag{9.8}$$

$$\Phi_{2,i} = \frac{2\pi}{\lambda_2}(\overline{n}_{c,i} - n_{m,2})d_i, \tag{9.9}$$

where λ_1 and λ_2 are the wavelengths of the light source.

By solving this system of equations, we obtain $\overline{n}_{c,i}$ and d_i for each pixel i. We have considered two different approaches to modify n_m: The first approach requires sequentially perfusing a standard cell perfusion solution and a second solution with a different RI but with the same osmolarity (to avoid cell volume variation) to record the two corresponding holograms at a single wavelength ($\lambda_1 = \lambda_2$) [39]. Practically, this procedure has permitted us to quantitatively measure some highly relevant RBC parameters, including mean corpuscular volume and mean corpuscular hemoglobin concentration [157]. However, owing to the solution exchange time, this approach precludes the possibility to monitor dynamic changes of cell morphology and RI that occur during fast biological processes. To overcome these drawbacks, we have developed a second approach, dual-wavelength ($\lambda_1 \neq \lambda_2$) DHM (DW-DHM) [132], which exploits the dispersion of the extracellular medium that is enhanced by the use of an extracellular dye ($n_{m,1} = n_m(\lambda_1) \neq n_m(\lambda_2) = n_{m,2}$) to achieve separate measurements of the intracellular RI and the absolute cell volume in real time [168].

This approach has been successfully applied to study the osmotic water membrane permeability P_f – representing the water volume flux per unit of time per unit of membrane surface for a given applied osmotic gradient – by monitoring cell volume changes while retaining the cell functionality [169]. Table 9.1 contains P_f measurements based on the monitoring of absolute cell volume in a variety of cell types.

Water crosses membrane though several routes (simple diffusion through the lipid bilayer, transmembrane proteins, specialized water channels, aquaporins, AQP, etc.). As regards the results of Table 9.1, the high membrane water permeability of human RBCs is mainly determined by the endogenously expressed water channel AQP1. However, the RBC provides an example where the water transport mechanism can easily be altered by pharmacological inhibition of AQP1 with mercury chloride HgCl2, a potent, rapid inhibitor of AQP1. The high water permeability in astrocytes is usually attributed to the endogenously expressed water channel aquaporin AQP4 and it has been shown that astrocytes from AQP4 deficient mice show a seven-fold reduced osmotic water permeability. The quite high water permeability measured in primary cultures of neurons could result from an increased expression of specific solute transporters that exhibit an intrinsic water permeability.

Table 9.1 Osmotic challenge: Measured parameters in different cell types. CHO cells (n = 46), HEK cells (n = 14), neurons (n = 11) astrocytes (n = 19) and red blood cells (RBCs) (n = 22). P_f: osmotic water membrane permeability , V_0 : initial cell volume, A_0: initial cell surface, Π_i/Π_0 : The respective ratio of the initial osmolarity to the hypoosmotic osmolarity. Adapted from [170]

	V_0 [μm^3]	Π_i/Π_0	A_0 [μm^2]	P_f [10^{-3} cm s^{-1}]
CHOs	1160 ± 669	1.452	747 ± 340	165 ± 0.318
HEKs	1996 ± 562	1.667	676 ± 153	3.04 ± 0.87
Neurons	1671 ± 1162	1.452	475 ± 226	4.69 ± 2.89
Astrocytes	861 ± 324	1.452	475 ± 137	7.64 ± 3.54
RBCs	95 ± 48	1.553	129 ± 44	5.2 ± 2.9
RBCs/$HgCl_2$	101 ± 49	1.553	135 ± 45	1.5 ± 1.2

Otherwise, resulting from the linear relationship between the intracellular RI and the dry mass, as well as from a dry mass balance equation, it has been possible to determine the RI of the transmembrane flux n_f [170]. The high precision with which n_f can be determined provides us whether the transmembrane water flux is accompanied by solute transport and therefore leads to characterization of the involved transmembrane transport process. A sustained application of glutamate on astrocytes has permitted us to detect a dry mass accumulation in good agreement with the expected uptake of glutamate through a specific co-transport.

Consequently, P_f, n_f, as well as absolute cell volume, represent indices providing some highly relevant information about the different mechanisms involved in the transmembrane water movements and in the complex question of cell volume regulation.

9.4.5 Exploration of Neuronal Cell Dynamics

A distinct feature of the nervous tissue is the intricate network of synaptic connections among neurons of diverse phenotypes. Although initial connections are formed largely through molecular mechanisms there is little doubt that electrical activities, influencing neuronal function and connectivity on multiple time scales, as well as on multiple levels of specificity, play a pivotal role in the development and integrative functions of neural networks/circuits. Nevertheless, how electrical activity affects the structure and function of neuronal networks is very limited. Consequently, the development of techniques that allow the noninvasive resolution of local neuronal network activity is required.

With respect to the study of neuronal activity electrophysiological approaches, in particular, voltage clamp and patch-clamp techniques, have permitted a major breakthrough by setting a voltage across the neuronal membrane and directly measuring the current flowing through a single ion channel. The patch clamp is the gold standard for assessing ion channel function, allowing discrimination of ionic currents in the femtoampere (10^{-15} A) range and with microsecond time resolution.

However, the patch clamp is still a highly invasive, laborious process requiring precise micromanipulations and a high degree of operational skill, which generally restricts voltage recording to a limited number of cells that form a neuronal network. Optical techniques seem to be an ideal solution for measuring membrane potentials because these techniques are relatively

noninvasive and work at both low and high magnification. For instance, a calcium indicator used in combination with high-resolution 2P microscopy allows measurement of the spiking activity of hundreds, or even several thousand, neurons in mammalian circuits while still keeping track of the activity of each neuron individually [171,172]. However, calcium imaging has its shortcomings and cannot substitute for voltage imaging [172].

Practically, voltage imaging methods have lagged behind calcium imaging as a result of important challenges related to physical constraints of the measurement themselves, including an electrical field closely located to the thin membrane region, an essentially two-dimensional plasma membrane that cannot contain an arbitrary number of voltage chromophores without disrupting its properties, and a plasma membrane representing only a small proportion of the total membrane surface in the neuron on which chromophores are attached. Finally, the relatively high speed of the electrical responses of mammalian neurons is also a serious challenge for voltage measurements.

Consequently, despite some promising features, the different voltage imaging methods suffer from poor signal-to-noise ratios and secondary side effects, and they fall short of providing single-cell resolution when imaging the activity of neuronal populations [172].

9.4.5.1 Measurement of Transmembrane Water Movements to Resolve Neuronal Network Activity

It is well known that neuronal activity induces modifications of intrinsic optical properties at the subcellular [173–176] cellular [177,178] and tissue levels [179–181]. Thus, we have studied the early stage of neuronal responses, induced by glutamate (the main excitatory neurotransmitter in the brain that is released in 80% of synapses), with multimodality microscopes, combining either DH-QPM with epifluorescence microscopy [182] or DH-QPM with electrophysiology [41], thereby allowing simultaneous monitoring of the DHM quantitative phase signal and the dynamics of intracellular ionic homeostasis or transmembrane ionic currents. Practically, experiments combining electrophysiology and DH-QPM, performed in a well-established biological model, allowed us to accurately study the relationship between transmembrane ionic currents and water movements. Concretely a mathematical relationship, involving some cell morphology parameters and a parameter ε (ml C^{-1}) representing the volume of the water movement associated with the net charge transported through the cell membrane, has been established between net transmembrane currents and the phase signals, thus opening the possibility of performing simultaneous multiple-site optical recording of transmembrane currents with DH-QPM [41].

Glutamate is known to induce an early neuronal swelling and to activate specific ionotropic receptors, namely the *N*-methyl-D-aspartate (NMDA), the 2-amino-3-(3-hydroxy-5-methyl-isoxazol-4-yl) propionate (AMPA), and the kainate receptors, which induce the opening of their associated ion channels, allowing influxes of Ca^{2+} and Na^{+} down their electrochemical gradient. Concretely, following various applications of glutamate in primary cultures of mouse cortical neurons, the multimodality DH-QPM electrophysiology setup recorded both a strong inward current and a decrease in phase signal, the amplitude of which was proportional to the concentration of glutamate and to the duration of the application. This inward current is consistent with glutamate-mediated activation of ionotropic receptors, and the phase decrease results from the dilution of the intracellular RI due to the osmotic water entry accompanying the net ionic influx, leading to the expected neuronal swelling. The receptor-specific

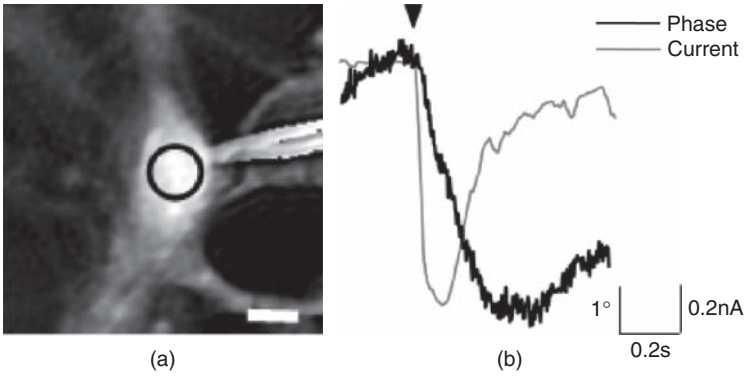

Figure 9.3 *Phase shift associated with glutamate-mediated neuronal activity*. (a) Quantative phase image of a patched mouse cortical neuron in primary culture recorded by DHM. The full circles in the middle of the cell correspond to the region of interest where the phase signal is recorded (scale bar: 10 μm). (B) Local application of glutamate (500 μM, 200 ms; arrow head) on the neuron triggered both a strong transient decrease of the phase signal associated to an inward current. Phase is expressed in degrees. *Source*: Marquet, P., Depeursinge, C., Magistretti, P.J., 2013, Neural cell dynamics explored with digital holographic microscopy, Annual Review of Biomedical Engineering, (15), 407–431

nature of these phase signals has been demonstrated by their suppression in the presence of MK801 and CNQX, two specific antagonists of NMDA and AMPA/kainate ionotropic receptors, respectively. Consequently these experiments have revealed that transmembrane water movements are one of the mechanisms inducing activity-related modifications of the intrinsic optical properties of neuronal cells. Actually, DH-QPM showed that glutamate produces mainly three distinct optical responses in neurons, which are predominantly mediated by NMDA receptors: biphasic, reversible decrease (RD), and irreversible decrease (ID) responses. The shape and amplitude of the optical signal were not associated with a particular neuronal phenotype but reflected the physiopathological status of neurons linked to the degree of NMDA activity [40]. These different phase responses can be separated into two components: a rapid one accompanying glutamate-mediated current (I_{GLUT}), the phase decrease depicted in Fig. 9.3, and a slow one corresponding generally to a phase recovery or a phase plateau (ID responses) when $I_{GLUT} = 0$. The phase recovery, which is much slower than the fast component, is likely to correspond to a nonelectrogenic neuronal volume regulation involving several mechanisms. Actually, furosemide and bumetanide, two inhibitors of sodium-coupled and/or potassium-coupled chloride movements, strongly modified the phase recovery, suggesting an involvement of two neuronal cotransporters, NKCC1 (Na-K-Cl) and KCC2 (K-Cl), in the optical response. This observation is of particular interest because it shows that DH-QPM is the first imaging technique able to monitor dynamically and in situ the activity of these nonelectrogenic co-transporters under physiological and/or pathological neuronal conditions [40]. Interestingly, the time course presented in Fig. 9.3 shows that the water movements are not significantly delayed, at the tenth-of-a-second scale at least, relative to the recorded current.

The measurement of I_{GLUT} as well as the concomitant rapid phase decrease corresponding to the early neuronal swelling allowed the estimation of the parameter $\varepsilon_{\mathrm{GLUT}}$ (ml C^{-1}). Practically, values of ε_{GLUT} lie within the range of 60–120 μm^3 nC^{-1}, equivalent to 340–620

water molecules transported per ion having crossed the membrane. The typical intracelluar RI change induced by a glutamate pulse (500 uM, 0.2 s) is around 0.002–0.003 corresponding to a substantial variation (7–10%) of the scattering potential proportional to the parameter $(\overline{n}_c^2 - n_m^2)$ and from which the scattering coefficient can be evaluated. The associated neuronal swelling is around 100 fL for a typical neuronal cell body of 1500 fL, corresponding to a 6–7% cell volume variation. It should be mentioned that these orders of magnitude correspond to an exogenous glutamate application during a few tenths of a second. Physiological release of endogenous glutamate could possibly induce smaller water movements and intracellular RI changes. Moreover, the mechanisms underlying these early significant and rapid fluxes of water, in contrast to those occurring during the phase recovery, remain to be clarified.

9.5 Future Issues

Holography has found an attractive field of application in microscopy. Because of its flexibility, DHM could easily be adapted to the need of microscopists and biologists. Complex wavefront reconstruction yields quantitative phase and accuracies in the nanometer, or even in the subnanometer range, with some statistical treatment, can be obtained. A major advantage of the holographic approach is that in-depth reconstruction and imaging is possible from a single hologram that can be acquired in a very short time interval.

As illustrated through these various applications, DH-QPM is well adapted to quantitatively study cell structure and dynamics. In practice, low energy levels and short exposure times are required to prevent photodamage, even during long experiments. In addition, DHM, as a label-free technique, does not require any solution change or insertion of dye, providing efficient conditions for high-throughput screening. However, although the quantitative phase signal provides unique information with high sensitivity about cell morphology and content, its interpretation in terms of biophysical parameters for analyzing specific biological mechanisms remains a major issue. Consequently, as has been illustrated with the decoupling procedures, any developments allowing us to separately measure the information corresponding to cell morphology and to cell content from the phase signal will represent an important step toward addressing some relevant biological questions. Within this framework, the development of a real time DHM-based optical diffraction tomography, by enabling both a direct access to the 3D RI map and to synthesize an enlarged numerical aperture (NA) providing super-resolved phase images represents a very promising way forward [183–188]. Indeed, future developments allowing high-resolution 3D mapping of the intracellular RI, could provide invaluable information about cytoarchitecture and compartmentalization of cytoplasm, which plays a critical role in several fundamental cell mechanisms, including protein synthesis.

On the other hand, integrating DH-QPM into a multimodal microscope is able to provide various different types of information on the cell state, also represent a promising way to obtain a comprehensive understanding of cell structure and dynamics. For instance multimodality approaches, combining DH-QPM with epifluorescence microscopy and/or with electrophysiology recordings have permitted us to efficiently explore the mechanisms underlying the complex processes of cell volume regulation, ion homeostasis, and transmembrane water movements, as well as their involvements in neuronal activity.

Acknowledgments

This article is the result of a close collaboration between the Microvision and Microdiagnosis Group (SCI/STI/CHD group) of EPFL with Florian Charrière, Jonas Kühn, Nicolas Pavillon, Etienne Shafer, and Yann Cotte; the Laboratory of Neuroenergetics and Cellular Dynamics at Brain and Mind Institute of EPFL with Benjamin Rappaz and Pascal Jourdain; the Center for Psychiatric Neuroscience at CHUV with Daniel Boss; and Lyncée Tec SA (www.lynceetec.com) with Etienne Cuche, Tristan Colomb, Frederic Montfort, Nicolas Aspert, and Yves Emery. We thank the Swiss National Science Foundation (SNSF grant CR3213_132993) for its support.

References

[1] Zernike F. 1942. Phase contrast, a new method for the microscopic observation of transparent objects. *Physica* **9**:686–6898.
[2] Barer R. 1952. Interference microscopy and mass determination. *Nature (London)* **169**:366–367.
[3] Dunn GA, Zicha D. 1993. Phase-shifting interference microscopy applied to the analysis of cell behavior. *Sym Soc Exp Biol* **47**:91–106.
[4] Gabor D. 1948. A new microscopic principle. *Nature* **161**:777–778.
[5] Conchello JA, Lichtman JW. 2005. Optical sectioning microscopy. *Nat Methods* **2**:920–931.
[6] Giepmans BN, Adams SR, Ellisman MH, Tsien RY. 2006. The fluorescent toolbox for assessing protein location and function. *Science* **312**:217–224.
[7] Campagnola P. 2011. Second harmonic generation imaging microscopy: applications to diseases diagnostics. *Anal Chem* **83**:3224–3231.
[8] Fujita K, Smith NI. 2008. Label-free molecular imaging of living cells. *Molecules and cells* **26**:530-5.
[9] Schermelleh L, Heintzmann R, Leonhardt H. 2010 A guide to super-resolution fluorescence microscopy. *J Cell Biol* **190**:165–175.
[10] Gould TJ, Hess ST, Bewersdorf J. 2012 Optical nanoscopy: from acquisition to analysis. *Annu Rev Biomed Eng* **14**:231–254.
[11] Indebetouw G, Klysubun P. 2001. Spatiotemporal digital microholography. *J Opt Soc Am A* **18**:319–325.
[12] Klysubun P, Indebetouw G. 2001. A posteriori processing of spatiotemporal digital microholograms. *J Opt Soc Am A* **18**:326–331.
[13] Cuche E, Marquet P, Depeursinge C. 1999. Simultaneous amplitude-contrast and quantitative phase-contrast microscopy by numerical reconstruction of Fresnel off-axis holograms. *Appl Optics* **38**:6994–7001.
[14] Yamaguchi I, Zhang T. 1997. Phase-shifting digital holography. *Opt Lett* **22**:1268–1270.
[15] Marquet P, Rappaz B, Magistretti PJ, Cuche E, Emery Y, *et al*. 2005. Digital holographic microscopy: a noninvasive contrast imaging technique allowing quantitative visualization of living cells with subwavelength axial accuracy. *Opt Lett* **30**:468–470.
[16] Mihailescu M, Scarlat M, Gheorghiu A, Costescu J, Kusko M, *et al*. 2011. Automated imaging, identification, and counting of similar cells from digital hologram reconstructions. *Appl Optics* **50**:3589–3597.
[17] Molder A, Sebesta M, Gustafsson M, Gisselson L, Wingren AG, Alm K. 2008. Non-invasive, label-free cell counting and quantitative analysis of adherent cells using digital holography. *Journal of Microscopy* **232**:240–247.
[18] DaneshPanah M, Zwick S, Schaal F, Warber M, Javidi B, Osten W. 2010. 3D holographic imaging and trapping for non-invasive cell identification and tracking. *J Disp Technol* **6**:490–499.

[19] Moon I, Javidi B, Yi F, Boss D, Marquet P. 2012. Automated statistical quantification of three-dimensional morphology and mean corpuscular hemoglobin of multiple red blood cells. *Opt Express* **20**:10295–10309.
[20] Crha I, Zakova J, Huser M, Ventruba P, Lousova E, Pohanka M. 2011. Digital holographic microscopy in human sperm imaging. *J Assist Reprod Gen* **28**:725–729.
[21] Liu R, Dey DK, Boss D, Marquet P, Javidi B. 2011. Recognition and classification of red blood cells using digital holographic microscopy and data clustering with discriminant analysis. *J Opt Soc Am A* **28**:1204–1210.
[22] Memmolo P, Di Caprio G, Distante C, Paturzo M, Puglisi R, *et al*. 2011. Identification of bovine sperm head for morphometry analysis in quantitative phase-contrast holographic microscopy. *Opt Express* **19**:23215-26.
[23] Janeckova H, Vesely P, Chmelik R. 2009. Proving tumour cells by acute nutritional/energy deprivation as a survival threat: a task for microscopy. *Anticancer Res* **29**:2339–2345.
[24] Mann CJ, Yu LF, Lo CM, Kim MK. 2005. High-resolution quantitative phase-contrast microscopy by digital holography. *Opt Express* **13**:8693–8698.
[25] Choi YS, Lee SJ. 2009. Three-dimensional volumetric measurement of red blood cell motion using digital holographic microscopy. *Appl Optics* **48**:2983–2990.
[26] Langehanenberg P, Ivanova L, Bernhardt I, Ketelhut S, Vollmer A, *et al*. 2009. Automated three-dimensional tracking of living cells by digital holographic microscopy. *J Biomed Opt* **14**:014018.
[27] Toy MF, Richard S, Kuhn J, Franco-Obregon A, Egli M, Depeursinge C. 2012. Digital holographic microscopy for the cytomorphological imaging of cells under zero gravity. *Three-Dimensional and Multidimensional Microscopy: Image Acquisition and Processing XIX*, p. 8227.
[28] Antkowiak M, Callens N, Yourassowsky C, Dubois F. 2008. Extended focused imaging of a microparticle field with digital holographic microscopy. *Opt Lett* **33**:1626–1628.
[29] Colomb T, Pavillon N, Kuhn J, Cuche E, Depeursinge C, Emery Y. 2010. Extended depth-of-focus by digital holographic microscopy. *Opt Lett* **35**:1840–1842.
[30] McElhinney C, Bryan Hennelly, Naughton T. 2008. Extended focused imaging for digital holograms of macroscopic three-dimensional objects. *Appl Optics* **47**:D71–D79.
[31] Warnasooriya N, Joud F, Bun P, Tessier G, Coppey-Moisan M, *et al*. 2010. Imaging gold nanoparticles in living cell environments using heterodyne digital holographic microscopy. *Opt Express* **18**:3264–3273.
[32] Bohm M, Mastrofrancesco A, Weiss N, Kemper B, von Bally G, *et al*. 2011. PACE4, a member of the prohormone convertase family, mediates increased proliferation, migration and invasiveness of melanoma cells in vitro and enhanced subcutaneous tumor growth in vivo. *J Invest Dermatol* **131**:S108.
[33] Dubois F, Yourassowsky C, Monnom O, Legros JC, Debeir O, *et al*. 2006. Digital holographic microscopy for the three-dimensional dynamic analysis of in vitro cancer cell migration. *J Biomed Opt* **11**:054032 (5 pages).
[34] Sun H, Song B, Dong H, Reid B, Player MA, *et al*. 2008. Visualization of fast-moving cells in vivo using digital holographic video microscopy. *J Biomed Opt* **13**:014007–014009.
[35] DaneshPanah M, Javidi B. 2007. Tracking biological microorganisms in sequence of 3D holographic microscopy images. *Opt Express* **15**:10761–10766.
[36] Rappaz B, Cano E, Colomb T, Kuhn J, Depeursinge C, *et al*. 2009. Noninvasive characterization of the fission yeast cell cycle by monitoring dry mass with digital holographic microscopy. *J Biomed Opt* **14**:034049.
[37] Rappaz B, Barbul A, Hoffmann A, Boss D, Korenstein R, *et al*. 2009. Spatial analysis of erythrocyte membrane fluctuations by digital holographic microscopy. *Blood Cell Mol Dis* **42**:228–232.
[38] Cardenas N, Yu LF, Mohanty SK. 2011. Stretching of red blood cells by optical tweezers quantified by digital holographic microscopy. *Optical Interactions with Tissue and Cells XXII* p. 7897.

[39] Rappaz B, Marquet P, Cuche E, Emery Y, Depeursinge C, Magistretti PJ. 2005. Measurement of the integral refractive index and dynamic cell morphometry of living cells with digital holographic microscopy. *Opt Express* **13**:9361–9373.

[40] Jourdain P, Pavillon N, Moratal C, Boss D, Rappaz B, *et al*. 2011. Determination of transmembrane water fluxes in neurons elicited by glutamate ionotropic receptors and by the cotransporters KCC2 and NKCC1: A digital holographic microscopy study. *J Neurosci* **31**:11846–11854.

[41] Jourdain P, Boss D, Rappaz B, Moratal C, Hernandez MC, *et al*. 2012. Simultaneous optical recording in multiple cells by digital holographic microscopy of chloride current associated to activation of the ligand-gated chloride channel GABA(A) receptor. *PloS One* **7**:e51041.

[42] Popescu G, Ikeda T, Best CA, Badizadegan K, Dasari RR, Feld MS. 2005. Erythrocyte structure and dynamics quantified by Hilbert phase microscopy. *J Biomed Opt* **10**:060503.

[43] Veselov O, Lekki J, Polak W, Strivay D, Stachura Z, *et al*. 2005. The recognition of biological cells utilizing quantitative phase microscopy system. *Nucl Instrum Meth B* **231**:212–217.

[44] Indebetouw G, Tada Y, Leacock J. 2006. Quantitative phase imaging with scanning holographic microscopy: an experimental assessment. *Biomed Eng Online* **5**.

[45] Amin MS, Park Y, Lue N, Dasari RR, Badizadegan K, *et al*. 2007. Microrheology of red blood cell membranes using dynamic scattering microscopy. *Opt Express* **15**:17001–17009.

[46] Fang-Yen C, Oh S, Park Y, Choi W, Song S, *et al*. 2007. Imaging voltage-dependent cell motions with heterodyne Mach–Zehnder phase microscopy. *Opt Lett* **32**:1572–1574.

[47] Park Y, Popescu G, Badizadegan K, Dasari RR, Feld MS. 2007. Fresnel particle tracing in three dimensions using diffraction phase microscopy. *Opt Lett* **32**:811–813.

[48] Whelan MP, Lakestani F, Rembges D, Sacco MG. 2007. Heterodyne interference microscopy for non-invasive cell morphometry – art. no. 66310E. *Novel Optical Instrumentation for Biomedical Applications III* **6631**:E6310.

[49] Brazhe AR, Brazhe NA, Rodionova NN, Yusipovich AI, Ignatyev PS, *et al*. 2008. Non-invasive study of nerve fibres using laser interference microscopy. *Philos T R Soc A* **366**:3463–3481.

[50] Lue N, Choi W, Badizadegan K, Dasari RR, Feld MS, Popescu G. 2008. Confocal diffraction phase microscopy of live cells. *Opt Lett* **33**:2074–2076.

[51] Pavani SRP, Libertun AR, King SV, Cogswell CJ. 2008. Quantitative structured-illumination phase microscopy. *Appl Optics* **47**:15–24.

[52] Popescu G, Park Y, Choi W, Dasari RR, Feld MS, Badizadegan K. 2008. Imaging red blood cell dynamics by quantitative phase microscopy. *Blood Cell Mol Dis* **41**:10–16.

[53] Tychinsky VP, Kretushev AV, Klemyashov IV, Vyshenskaya TV, Filippova NA, *et al*. 2008. Quantitative real-time analysis of nucleolar stress by coherent phase microscopy. *J Biomed Opt* **13**:064032.

[54] Warger WC, DiMarzio CA. 2008. Modeling of optical quadrature microscopy for imaging mouse embryos – art. no. 68610T. In *Three-Dimensional and Multidimensional Microscopy: Image Acquisition and Processing XV*, eds JA Conchello, CJ Cogswell, T Wilson, TG Brown, **6861**:T8610-T.

[55] Lee S, Lee JY, Yang W, Kim DY. 2009. The measurement of red blood cell volume change induced by Ca(2+) based on full field quantitative phase microscopy. *Imaging, Manipulation, and Analysis of Biomolecules, Cells, and Tissues VII*, p. 7182.

[56] Park Y, Yamauchi T, Choi W, Dasari R, Feld MS. 2009. Spectroscopic phase microscopy for quantifying hemoglobin concentrations in intact red blood cells. *Opt Lett* **34**:3668–3670.

[57] Shaked NT, Zhu YZ, Rinehart MT, Wax A. 2009. Two-step-only phase-shifting interferometry with optimized detector bandwidth for microscopy of live cells. *Opt Express* **17**:15585–15591.

[58] Moradi AR, Ali MK, Daneshpanah M, Anand A, Javidi B. 2010. Detection of calcium-induced morphological changes of living cells using optical traps. *IEEE Photonics J* **2**:775–783.

[59] Shaked NT, Finan JD, Guilak F, Wax A. 2010. Quantitative phase microscopy of articular chondrocyte dynamics by wide-field digital interferometry. *J Biomed Opt* **15**(1):010505.
[60] Tychinsky VP, Tikhonov AN. 2010. Interference microscopy in cell biophysics. 2. Visualization of individual cells and energy-transducing organelles. *Cell Biochem Biophys* **58**:117–128.
[61] Wang P, Bista RK, Khalbuss WE, Qiu W, Uttam S, *et al*. 2010. Nanoscale nuclear architecture for cancer diagnosis beyond pathology via spatial-domain low-coherence quantitative phase microscopy. *J Biomed Opt* **15**:066028.
[62] Xue L, Lai JC, Li ZH. 2010. Quantitative phase microscopy of red blood cells with slightly-off-axis interference. *Optics in Health Care and Biomedical Optics IV* **7845**:784505–784508.
[63] Yamauchi T, Sugiyama N, Sakurai T, Iwai H, Yamashita Y. 2010. Label-free classification of cell types by imaging of Cell Membrane Fluctuations Using Low-Coherent Full-Field Quantitative Phase Microscopy. *Three-Dimensional and Multidimensional Microscopy: Image Acquisition and Processing XVII* **7570**:75700X-X-8.
[64] Yang W, Lee S, Lee J, Bae Y, Kim D. 2010. Silver nanoparticle-induced degranulation observed with quantitative phase microscopy. *J Biomed Opt* **15**:045005.
[65] Gonzalez-Laprea J, Marquez A, Noris-Suarez K, Escalona R. 2011. Study of bone cells by quantitative phase microscopy using a Mirau interferometer. *Rev Mex Fis* **57**:435–440.
[66] Lee S, Kim YR, Lee JY, Rhee JH, Park CS, Kim DY. 2011. Dynamic analysis of pathogen-infected host cells using quantitative phase microscopy. *J Biomed Opt* **16**:036004.
[67] Kim M, Choi Y, Fang-Yen C, Sung YJ, Dasari RR, *et al*. 2011. High-speed synthetic aperture microscopy for live cell imaging. *Opt Lett* **36**:148–150.
[68] Lee S, Lee JY, Park CS, Kim DY. 2011. Detrended fluctuation analysis of membrane flickering in discocyte and spherocyte red blood cells using quantitative phase microscopy. *J Biomed Opt* **16**:076009.
[69] Park YK, Best CA, Auth T, Gov NS, Safran SA, *et al*. 2010. Metabolic remodeling of the human red blood cell membrane. *P Natl Acad Sci USA* **107**:1289–1294.
[70] Wang P, Bista R, Bhargava R, Brand RE, Liu Y. 2011. Spatial-domain Low-coherence Quantitative Phase Microscopy for Cancer Diagnosis. *Optical Coherence Tomography and Coherence Domain Optical Methods in Biomedicine XV* **7889**.
[71] Wang R, Ding HF, Mir M, Tangella K, Popescu G. 2011. Effective 3D viscoelasticity of red blood cells measured by diffraction phase microscopy. *Biomed Opt Express* **2**:485–490.
[72] Yamauchi T, Iwai H, Yamashita Y. 2011. Label-free imaging of intracellular motility by low-coherent quantitative phase microscopy. *Opt Express* **19**:5536–5550.
[73] Yaqoob Z, Yamauchi T, Choi W, Fu D, Dasari RR, Feld MS. 2011. Single-shot full-field reflection phase microscopy. *Opt Express* **19**:7587–7595.
[74] Ansari R, Aherrahrou R, Aherrahrou Z, Erdmann J, Huttmann G, Schweikard A. 2012. Quantitative analysis of cardiomyocyte dynamics with optical coherence phase Microscopy. *Optical Coherence Tomography and Coherence Domain Optical Methods in Biomedicine Xvi* **8213**:821338.
[75] Cardenas N, Mohanty SK. 2012. Investigation of shape memory of red blood cells using optical tweezers and quantitative phase microscopy. *Imaging, Manipulation, and Analysis of Biomolecules, Cells, and Tissues X* **8225**:82252B.
[76] Pan F, Liu S, Wang Z, Shang P, Xiao W. 2012. Dynamic and quantitative phase-contrast imaging of living cells under simulated zero gravity by digital holographic microscopy and superconducting magnet. *Laser Phys* **22**:1435–1438.
[77] Tychinsky VP, Kretushev AV, Vyshenskaya TV, Shtil AA. 2012. Dissecting eukaryotic cells by coherent phase microscopy: quantitative analysis of quiescent and activated T lymphocytes. *J Biomed Opt* **17**:076020.

[78] Yamauchi T, Sakurai T, Iwai H, Yamashita Y. 2012. Long-term measurement of spontaneous membrane fluctuations over a wide dynamic range in the living cell by low-coherent quantitative phase microscopy. *Imaging, Manipulation, and Analysis of Biomolecules, Cells, and Tissues X* **8225**:82250A.

[79] Curl CL, Bellair CJ, Harris PJ, Allman BE, Roberts A, *et al*. 2004. Quantitative phase microscopy: a new tool for investigating the structure and function of unstained live cells. *Clin Exp Pharmacol P* **31**:896–901.

[80] Almoro PF, Waller L, Agour M, Falldorf C, Pedrini G, *et al*. 2012. Enhanced deterministic phase retrieval using a partially developed speckle field. *Opt Lett* **37**:2088–2090.

[81] Bon P, Maucort G, Wattellier B, Monneret S. 2009. Quadriwave lateral shearing interferometry for quantitative phase microscopy of living cells. *Opt Express* **17**:13080–13094.

[82] Almoro PF, Pedrini G, Gundu PN, Osten W, Hanson SG. 2010. Phase microscopy of technical and biological samples through random phase modulation with a diffuser. *Opt Lett* **35**:1028–1030.

[83] Zhang Y, Pedrini G, Osten W, Tiziani HJ. 2004. Phase retrieval microscopy for quantitative phase-contrast imaging. *Optik* **115**:94–96.

[84] Chhaniwal VK, Anand A, Faridian A, Pedrini G, Osten W, Javidi B. 2011. Single beam quantitative phase contrast 3D microscopy of cells. *Proc Spie* 8092:80920D-D-8.

[85] Bao P, Situ G, Pedrini G, Osten W. 2012. Lensless phase microscopy using phase retrieval with multiple illumination wavelengths. *Appl Optics* **51**:5486–5494.

[86] Cogswell CJ, Smith NI, Larkin KG, Hariharan P. 1997. Quantitative DIC microscopy using a geometric phase shifter. *Three-Dimensional Microscopy: Image Acquisition and Processing IV, Proceedings of* **2984**:72–81.

[87] Ishiwata H, Yatagai T, Itoh M, Tsukada A. 1999. Quantitative phase analysis in retardation modulated differential interference contrast (RM-DIC) microscope. *Interferometry '99: Techniques and Technologies* **3744**:183–187.

[88] Totzeck M, Kerwien N, Tavrov A, Rosenthal E, Tiziani HJ. 2002. Quantitative Zernike phase-contrast microscopy by use of structured birefringent pupil-filters and phase-shift evaluation. *P Soc Photo-Opt Ins* **4777**:1–11.

[89] King SV, Libertun A, Piestun R, Cogswell CJ, Preza C. 2008. Quantitative phase microscopy through differential interference imaging. *J Biomed Opt* **13**:024020.

[90] Kou SS, Waller L, Barbastathis G, Sheppard CJR. 2010. Transport-of-intensity approach to differential interference contrast (TI-DIC) microscopy for quantitative phase imaging. *Opt Lett* **35**:447–449.

[91] Fu D, Oh S, Choi W, Yamauchi T, Dorn A, *et al*. 2010. Quantitative DIC microscopy using an off-axis self-interference approach. *Opt Lett* **35**:2370–2302.

[92] Gao P, Yao BL, Harder I, Lindlein N, Torcal-Milla FJ. 2011. Phase-shifting Zernike phase contrast microscopy for quantitative phase measurement. *Opt Lett* **36**:4305–4307.

[93] Pavillon N. 2011. *Cellular dynamics and three-dimensional refractive index distribution studied with quantitative phase imaging* (Doctoral dissertation).

[94] Gabor D. 1948. A new microscopic principle. *Nature* **161**:777.

[95] Gabor D. 1949. Microscopy by reconstructed wave-fronts. *Proceedings of the Royal Society of London. Serie A*, *Mathematical and Physical Sciences* **197**:454–487.

[96] Leith EN, Upatnieks J. 1964. Wavefront reconstruction with diffused illumination and three-dimensional objects. *J Opt Soc Am* **54**:1295–1301.

[97] Leith EN, Upatniek.J. 1962. Reconstructed wavefronts and communication theory. *J Opt Soc Am* **52**:1123.

[98] Wolf E, Shewell JR. 1970. Diffraction theory of holography. *J Math Phys* **11**:2254.

[99] Carter WH. 1970. Computational reconstruction of scattering objects from holograms. *J Opt Soc Am* **60**:306–314.

[100] Dubois F, Callens N, Yourassowsky C, Hoyos M, Kurowski P, Monnom O. 2006. Digital holographic microscopy with reduced spatial coherence for three-dimensional particle flow analysis. *Appl Optics* **45**:864–871.
[101] Kemper B, Stürwald S, Remmersmann C, Langehanenberg P, von Bally G. 2008. Characterisation of light emitting diodes (LEDs) for application in digital holographic microscopy for inspection of micro and nanostructured surfaces. *Opt Laser Eng* **46**:499–507.
[102] Ansari Z, Gu Y, Tziraki M, Jones R, French PMW, *et al*. 2001. Elimination of beam walk-off in low-coherence off-axis photorefractive holography. *Opt. Lett.* **26**:334–336.
[103] Goodman JW, Lawrence RW. 1967. Digital image formation from electronically detected holograms. *Applied Physics Letters* **11**:77–79.
[104] Schnars U, Jüptner W. 1994. Direct recording of holograms by a CCD target and numerical reconstruction. *Appl Optics* **33**:179–181.
[105] Coquoz O, Conde R, Taleblou F, Depeursinge C. 1995. Performances of endoscopic holography with a multicore optical-fiber. *Appl Optics* **34**:7186–7193.
[106] Bruning JH, Herriott DR, Gallaghe JE, Rosenfel DP, White AD, Brangacc DJ. 1974. Digital wavefront measuring interferometer for testing optical surfaces and lenses. *Appl Optics* **13**:2693–2703.
[107] Carré P. 1966. Installation et utilisation du comparateur photoélectrique et interférentiel du Bureau International des Poids et Mesures. *Metrologia* **2**:13–33.
[108] Kreis T. 2005. *Handbook of Holographic Interferometry: Optical and Digital Methods*. Weinheim, FRG: Wiley-VCH Verlag GmbH & Co. KGaA.
[109] Rastogi P. 1994. *Holographic Interferometry: Principles and Methods*. NY: Springer-Verlag.
[110] Guo P, Devaney AJ. 2004. Digital microscopy using phase-shifting digital holography with two reference waves. *Opt Lett* **29**:857–859.
[111] Liu JP, Poon TC. 2009. Two-step-only quadrature phase-shifting digital holography. *Opt Lett* **34**:250–252.
[112] Awatsuji Y, Sasada M, Kubota T. 2004. Parallel quasi-phase-shifting digital holography. *Applied Physics Letters* **85**:1069–1071.
[113] Guo CS, Zhang L, Wang HT, Liao J, Zhu YY. 2002. Phase-shifting error and its elimination in phase-shifting digital holography. *Opt Lett* **27**:1687–1689.
[114] Xu XF, Cai LZ, Wang YR, Meng XF, Sun WJ, *et al*. 2008. Simple direct extraction of unknown phase shift and wavefront reconstruction in generalized phase-shifting interferometry: algorithm and experiments. *Opt. Lett.* **33**:776–778.
[115] Wang Z, Han B. 2004. Advanced iterative algorithm for phase extraction of randomly phase-shifted interferograms. *Opt Lett* **29**:1671–1673.
[116] Schnars U, Juptner W. 1994. Direct recording of holograms by a CCD target and numerical reconstruction. *Appl Optics* **33**:179–181.
[117] Takeda M, Ina H, Kobayashi S. 1982. Fourier-transform method of fringe-pattern analysis for computer-based topography and interferometry. *J Opt Soc Am* **72**:156–160.
[118] Kreis T. 1986. Digital holographic interference-phase measurement using the Fourier-transform method. *Journal of the Optical Society of America A. Optics and Image Science* **3**:847–855.
[119] Cuche E, Poscio P, Depeursinge C. 1997. Optical tomography by means of a numerical low-coherence holographic technique. *Journal of Optics-Nouvelle Revue D Optique* **28**:260–264.
[120] Montfort F, Charrière F, Colomb T, Cuche E, Marquet P, Depeursinge C. 2006. Purely numerical compensation for microscope objective phase curvature in digital holographic microscopy: influence of digital phase mask position. *J Opt Soc Am A* **23**:2944–2953.
[121] Colomb T, Montfort F, Kühn J, Aspert N, Cuche E, *et al*. 2006. Numerical parametric lens for shifting, magnification and complete aberration compensation in digital holographic microscopy. *J Opt Soc Am A* **23**:3177–190.
[122] Colomb T, Kühn J, Charrière F, Depeursinge C, Marquet P, Aspert N. 2006. Total aberrations compensation in digital holographic microscopy with a reference conjugated hologram. *Opt Express* **14**:4300–4306.

[123] Colomb T, Cuche E, Charrière F, Kühn J, Aspert N, *et al*. 2006. Automatic procedure for aberration compensation in digital holographic microscopy and applications to specimen shape compensation. *Appl Optics* **45**:851–863.
[124] Colomb T, Charriere F, Kuhn J, Marquet P, Depeursinge C. 2008. Advantages of digital holographic microscopy for real-time full field absolute phase imaging – art. no. 686109. *Three-Dimensional and Multidimensional Microscopy: Image Acquisition and Processing XV* **6861**:86109.
[125] Ferraro P, Grilli S, Alfieri D, Nicola SD, Finizio A, *et al*. 2005. Extended focused image in microscopy by digital Holography. *Opt Express* **13**:6738–6749.
[126] Cuche E, Bevilacqua F, Depeursinge C. 1999. Digital holography for quantitative phase-contrast imaging. *Opt Lett* **24**:291–293.
[127] Haddad WS, Cullen D, Solem JC, Longworth JW, McPherson A, *et al*. 1992. Fourier-transform holographic microscope. *Appl Optics* **31**:4973–4978.
[128] Takaki Y, Kawai H, Ohzu H. 1999. Hybrid holographic microscopy free of conjugate and zero-order images. *Appl Optics* **38**:4990–4996.
[129] Xu W, Jericho MH, Meinertzhagendagger IA, Kreuzer HJ. 2001. Digital in-line holography for biological applications. *PNAS* **98**:11301–11305.
[130] Colomb T, Dahlgren P, Beghuin D, Cuche E, Marquet P, Depeursinge C. 2002. Polarization imaging by use of digital holography. *Appl Optics* **41**:27–37.
[131] Colomb T, Dürr F, Cuche E, Marquet P, Limberger H, *et al*. 2005. Polarization microscopy by use of digital holography: application to optical fiber birefringence measurements. *Appl Optics* **44**:4461–4469.
[132] Kuhn J, Colomb T, Montfort F, Charriere F, Emery Y, *et al*. 2007. Real-time dual-wavelength digital holographic microscopy with a single hologram acquisition. *Opt Express* **15**:7231–7242.
[133] Zhang T, Yamaguchi I. 1998. Three-dimensional microscopy with phase-shifting digital holography. *Opt Lett* **23**:1221–1223.
[134] Cuche E, Marquet P, Depeursinge C. 2000. Spatial filtering for zero-order and twin-image elimination in digital off-axis holography. *Appl Optics* **39**:4070–4075.
[135] Cuche E, Marquet P, Depeursinge C. 2000. Aperture apodization using cubic spline interpolation: application in digital holographic microscopy. *Opt Commun* **182**:59–69.
[136] Charriere F, Colomb T, Montfort F, Cuche E, Marquet P, Depeursinge C. 2006. Shot-noise influence on the reconstructed phase image signal-to-noise ratio in digital holographic microscopy. *Appl Optics* **45**:7667–7673.
[137] Charrière F, Rappaz B, Kühn J, Colomb T, Marquet P, Depeursinge C. 2007. Influence of shot noise on phase measurement accuracy in digital holographic microscopy. *Opt Express* **15**:8818–8831.
[138] Seo S, Isikman SO, Sencan I, Mudanyali O, Su TW, *et al*. 2010. High-throughput lens-free blood analysis on a chip. *Analytical Chemistry* **82**:4621–4627.
[139] Milgram JH, Li WC. 2002. Computational reconstruction of images from holograms. *Appl Optics* **41**:853–864.
[140] Yi F, Lee CG, Moon IK. 2012. Statistical analysis of 3D volume of red blood cells with different shapes via digital holographic microscopy. *J Opt Soc Korea* **16**:115–120.
[141] Moon I, Yi F, Javidi B. 2010. Automated three-dimensional microbial sensing and recognition using digital holography and statistical sampling. *Sensors-Basel* **10**:8437–8451.
[142] Javidi B, Daneshpanah M, Moon I. 2010. Three-dimensional holographic imaging for identification of biological micro/nanoorganisms. *IEEE Photonics J* **2**:256–259.
[143] Anand A, Chhaniwal VK, Javidi B. 2011. imaging embryonic stem cell dynamics using quantitative 3-D digital holographic microscopy. *IEEE Photonics J* **3**:546–554.

[144] Miccio L, Finizio A, Memmolo P, Paturzo M, Merola F, *et al*. 2011. Detection and visualization improvement of spermatozoa cells by digital holography. In *Molecular Imaging III*, eds CP Lin, V Ntziachristos, p. 8089.
[145] Antkowiak M, Callens N, Schockaert C, Yourassowsky C, Dubois F. 2008. Accurate three-dimensional detection of micro-particles by means of digital holographic microscopy – art. no. 699514. In *Optical Micro- and Nanometrology in Microsystems Technology II*, eds C Gorecki, AK Asundi, W Osten, **6995**:99514.
[146] Bae Y, Lee S, Yang W, Kim DY. 2010. Three-dimensional Single Particle Tracking using Off-axis Digital Holographic Microscopy. *Nanoscale Imaging, Sensing, and Actuation for Biomedical Applications VII* **7574**:757408.
[147] Hsieh CL, Grange R, Pu Y, Psaltis D. 2009. Three-dimensional harmonic holographic microcopy using nanoparticles as probes for cell imaging. *Opt Express* **17**:2880–2891.
[148] Shaffer E, Depeursinge C. 2010. Digital holography for second harmonic microscopy: application to 3D-tracking of nanoparticles. *Biophotonics: Photonic Solutions for Better Health Care II* **7715**.
[149] Mann CJ, Yu LF, Kim MK. 2006. Movies of cellular and sub-cellular motion by digital holographic microscopy. *Biomed Eng Online* **5**:21.
[150] Sun HY, Song B, Dong HP, Reid B, Player MA, *et al*. 2008. Visualization of fast-moving cells in vivo using digital holographic video microscopy. *J Biomed Opt* **13**:014007.
[151] Javidi B, Moon I, Daneshpanaha M. 2010. Detection, identification and tracking of biological micro/nano organisms by computational 3D optical imaging. *Biosensing III* **7759**:77590R-R-6.
[152] Barer R. 1953. Determination of dry mass, thickness, solid and water concentration in living cells. *Nature (London)* **172**:1097–1098.
[153] Popescu G, Park Y, Lue N, Best-Popescu C, Deflores L, *et al*. 2008. Optical imaging of cell mass and growth dynamics. *Am J Physiol-Cell Ph* **295**:C538–C544.
[154] Kemper B, Bauwens A, Vollmer A, Ketelhut S, Langehanenberg P, *et al*. 2010. Label-free quantitative cell division monitoring of endothelial cells by digital holographic microscopy. *J Biomed Opt* **15**:036009.
[155] Mir M, Wang Z, Shen Z, Bednarz M, Bashir R, *et al*. 2011. Optical measurement of cycle-dependent cell growth. *P Natl Acad Sci USA* **108**:13124–13129.
[156] Zicha D, Dunn GA. 1995. An image-processing system for cell behavior studies in subconfluent cultures. *J Microsc-Oxford* **179**:11–21.
[157] Rappaz B, Barbul A, Emery Y, Korenstein R, Depeursinge C, *et al*. 2008. Comparative study of human erythrocytes by digital holographic microscopy, confocal microscopy, and impedance volume analyzer. *Cytom Part A* **73A**:895–903.
[158] Yusipovich AI, Parshina EY, Brysgalova NY, Brazhe AR, Brazhe NA, *et al*. 2009. Laser interference microscopy in erythrocyte study. *J Appl Phys* **105**:102037.
[159] Pham H, Bhaduri B, Ding HF, Popescu G. 2012. Spectroscopic diffraction phase microscopy. *Opt Lett* **37**:3438–3440.
[160] Rinehart M, Zhu YZ, Wax A. 2012. Quantitative phase spectroscopy. *Biomed Opt Express* **3**:958–965.
[161] Jang Y, Jang J, Park Y. 2012. Dynamic spectroscopic phase microscopy for quantifying hemoglobin concentration and dynamic membrane fluctuation in red blood cells. *Opt Express* **20**:9673–9681.
[162] Boss D, Hoffmann A, Rappaz B, Depeursinge C, Magistretti PJ, *et al*. 2012. Spatially-resolved eigenmode decomposition of red blood cells membrane fluctuations questions the role of ATP in flickering. *Plos One* **7**:e40667.
[163] Mauritz JMA, Esposito A, Tiffert T, Skepper JN, Warley A, *et al*. 2010. Biophotonic techniques for the study of malaria-infected red blood cells. *Med Biol Eng Comput* **48**:1055–1063.

[164] Cardenas N, Yu LF, Mohanty SK. 2011. Probing orientation and rotation of red blood cells in optical tweezers by digital holographic microscopy. *Optical Diagnostics and Sensing Xi: Toward Point-of-Care Diagnostics and Design and Performance Validation of Phantoms Used in Conjunction with Optical Measurement of Tissue Iii* **7906**:790613–790619.
[165] Esseling M, Kemper B, Antkowiak M, Stevenson DJ, Chaudet L, *et al*. 2012. Multimodal biophotonic workstation for live cell analysis. *J Biophotonics* **5**:9–13.
[166] Lue N, Popescu G, Ikeda T, Dasari RR, Badizadegan K, Feld MS. 2006. Live cell refractometry using microfluidic devices. *Opt Lett* **31**:2759–2761.
[167] Kemper B, Kosmeier S, Langehanenberg P, von Bally G, Bredebusch I, *et al*. 2007. Integral refractive index determination of living suspension cells by multifocus digital holographic phase contrast microscopy. *J Biomed Opt* **12**:054009 (5 pages).
[168] Rappaz B, Charrière F, Depeursinge C, Magistretti PJ, Marquet P. 2008. Simultaneous cell morphometry and refractive index measurement with dual-wavelength digital holographic microscopy and dye-enhanced dispersion of perfusion medium. *Opt Lett* **33**:744–746.
[169] Boss D, Kuhn J, Jourdain P, Depeursinge C, Magistretti PJ, Marquet P. Measurement of absolute cell volume, osmotic membrane water permeability, and refractive index of transmembrane water and solute flux by digital holographic microscopy. *J Biomed Opt* **18**:036007.
[170] Boss D, Kuehn J, Jourdain P, Depeursinge C, Magistretti PJ, Marquet P. 2013. Measurement of absolute cell volume and osmotic water membrane permeability by real time dual wavelength holographic microscopy. *J Biomed Opt* in press.
[171] Cossart R, Aronov D, Yuste R. 2003. Attractor dynamics of network UP states in the neocortex. *Nature* **423**:283–288.
[172] Peterka DS, Takahashi H, Yuste R. 2011. Imaging voltage in neurons. *Neuron* **69**:9–21.
[173] Carter KM, George JS, Rector DM. 2004. Simultaneous birefringence and scattered light measurements reveal anatomical features in isolated crustacean nerve. *J Neurosci Methods* **135**:9–16.
[174] Cohen LB. 1973. Changes in neuron structure during action potential propagation and synaptic transmission. *Physiol Rev* **53**:373–418.
[175] Tasaki I, Watanabe A, Sandlin R, Carnay L. 1968. Changes in fluorescence, turbidity, and birefringence associated with nerve excitation. *Proc Natl Acad Sci U S A* **61**:883–888.
[176] Hill DK, Keynes RD. 1949. Opacity changes in stimulated nerve. *J Physiol* **108**:278–281.
[177] Tasaki I, Byrne PM. 1992. Rapid structural changes in nerve fibers evoked by electric current pulses. *Biochem Biophys Res Commun* **188**:559–564.
[178] Stepnoski RA, LaPorta A, Raccuia-Behling F, Blonder GE, Slusher RE, Kleinfeld D. 1991. Noninvasive detection of changes in membrane potential in cultured neurons by light scattering. *Proc Natl Acad Sci U S A* **88**:9382–9386.
[179] Holthoff K, Witte OW. 1996. Intrinsic optical signals in rat neocortical slices measured with near-infrared dark-field microscopy reveal changes in extracellular space. *J Neurosci* **16**:2740–2749.
[180] Andrew RD, Adams JR, Polischuk TM. 1996. Imaging NMDA- and kainate-induced intrinsic optical signals from the hippocampal slice. *J Neurophysiol* **76**:2707–2717.
[181] MacVicar BA, Hochman D. 1991. Imaging of synaptically evoked intrinsic optical signals in hippocampal slices. *J Neurosci* **11**:1458–1469.
[182] Pavillon N, Benke A, Boss D, Moratal C, Kuhn J, *et al*. 2010. Cell morphology and intracellular ionic homeostasis explored with a multimodal approach combining epifluorescence and digital holographic microscopy. *J Biophotonics* **3**:432–436.
[183] Charrière F, Marian A, Montfort F, Kühn J, Colomb T, *et al*. 2006. Cell refractive index tomography by digital holographic microscopy. *Opt Lett* **31**:178–810.
[184] Debailleul M, Georges V, Simon B, Morin R, Haeberle O. 2009. High-resolution three-dimensional tomographic diffractive microscopy of transparent inorganic and biological samples. *Opt Lett* **34**:79–81.

[185] Choi W, Fang-Yen C, Badizadegan K, Oh S, Lue N, *et al*. 2007. Tomographic phase microscopy. *Nat Methods* **4**:717–719.

[186] Sheppard CJR, Kou SS. 2010. 3D imaging with holographic tomography. *International Conference on Advanced Phase Measurement Methods in Optics an Imaging* **1236**:65–69.

[187] Park Y, Diez-Silva M, Fu D, Popescu G, Choi W, *et al*. 2010. Static and dynamic light scattering of healthy and malaria-parasite invaded red blood cells. *J Biomed Opt* **15**:020506.

[188] Cotte Y, Toy FM, Jourdain P, Pavillon N, Boss D, *et al*. 2013. Marker-free phase nanoscopy. *Nature Photonics* **7**, 113–117.